Fourier-Series-Based Phase Delay Compensation of Brushless DC Motor Systems

Myougseok Lee, *Student Member, IEEE*, and Kyoungchul Kong, *Member, IEEE*

***Abstract*—Brushless direct-current (BLDC) motors are being regarded as a standard of actuation methods for precise and heavy-duty applications, such as robots and vehicles. To improve the efficiency and torque performance of the BLDC motors, various design parameters (e.g., the magnetic flux density, core material, etc.) have been investigated. Phase delay compensation (PDC), also often called phase advance angle control, is also an attractive method that improves the actuation efficiency of BLDC motors without any mechanical modification of the motors. Due to the inductance of the BLDC motor windings, the magnetic flux of a rotor and that of a stator are not generated in phase, which causes a phase delay in magnetization of the coil. Due to this phenomenon, the efficiency of the BLDC motor is remarkably decreased, in particular at a high speed, and the PDC can be applied to compensate for this phase delay. In this paper, Fourier-series-based PDC is proposed to improve the efficiency of the motor; the phase delay angle is calculated based on the dynamic model of the motor windings and its Fourier series. The proposed Fourier-series-based PDC is realized by designing an inverter circuit that switches the phase voltages according to the proposed algorithm. The performance of PDC is verified at experiments in terms of not only T–N curve but also control performance. According to the experimental results, PDC improves output torque, efficiency, and control performance.**

***Index Terms*—Brushless dc motor, motor driver, phase current delay, phase delay compensator (PDC).**

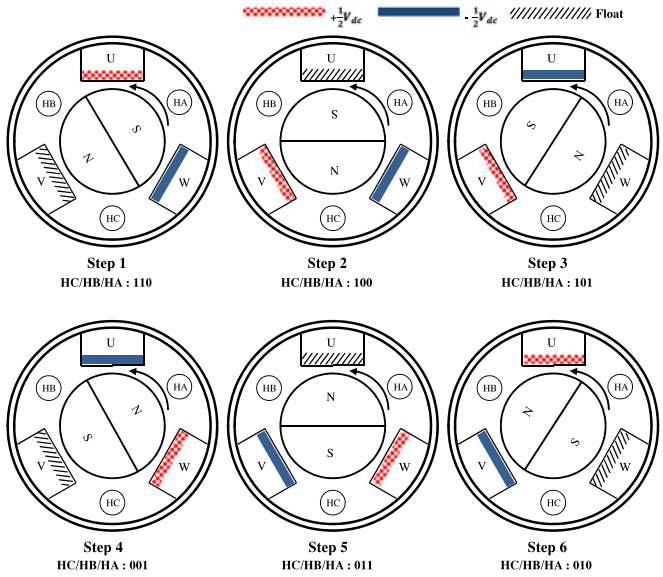

Fig. 1. Two-phase excitation method with six steps for driving three-phase BLDC motors. HA, HB, and HC represent the hall sensors located at the three positions.

I. Introduction

PERMANENT magnet brushless direct-current (BLDC) motors have various advantageous characteristics, such as high efficiency, high power density, and high speed operation range. In addition, compared to conventional brushed dc motors that include the mechanical contact structure of a commutator and brushes, the BLDC motors generate lesser electromagnetic and mechanical noises and show better durability due to the absence of the mechanical contact. Therefore, they have been widely used, such as home appliances, electronic products, vehicles, industrial machinery, and medical devices [1]–[5]. While the electric phase current is mechanically and automatically switched in the brushed dc motors, BLDC motors often require position sensors, such as hall sensors, to obtain the position information for synchronization between a magnet and the magnetic field by a coil. In particular, the three-phase BLDC motors, which are the most common BLDC motors, are driven according to the six steps of the rotor positions distinguished from the hall sensor signals as shown in Fig. 1; for the continuous rotation of a rotor, a stator should be alternately magnetized by the current drive circuit of an inverter that switches phase currents according to the hall sensor signals. A two-phase excitation method, in which two phases are excited whereas the remaining one phase is floating, is the most commonly used for driving the three-phase BLDC motors [6]. In the two-phase excitation method, it is assumed that the detection of the hall sensor signals and the phase transition occur at the same time. In practice, however, the phase current is delayed from the phase transition instance due to the commutation scheme of BLDC motor [7], [8], and the inductance of motor windings [9]. Especially, the larger inductance of windings and the higher operation speed, the more delayed phase current. This problem may considerably deteriorate the performance of BLDC motors, such as the output torque and efficiency reduction at a high speed [10], [22]. Consequently, the operation range of

Manuscript received October 23, 2016; revised December 29, 2016; accepted January 31, 2017. Date of publication February 14, 2017; date of current version October 6, 2017. This work was supported by the Basic Science Research Program through the National Research Foundation of South Korea (NRF) funded by the Ministry of Science, ICT, and Future Planning (NRF-2015R1A1A1A05001448). Recommended for publication by Associate Editor J. Hur.

The authors are with the Department of Mechanical Engineering, Sogang University, Seoul 121-742, South Korea (e-mail: jeff0115@sogang.ac.kr; kckong@sogang.ac.kr).

Color versions of one or more of the figures in this paper are available online at http://ieeexplore.ieee.org.

Digital Object Identifier 10.1109/TPEL.2017.2669040

BLDC motors is reduced, and the efficiency at a high speed is lowered.

Phase delay compensation (PDC), which is also often called phase advance angle control, has been studied to solve the phase delay problem in BLDC motor systems; it is to compensate for the phase delay caused by the inductance of motor windings. The improved torque and speed performances of BLDC motors by the PDC have long been verified through extensive simulations and experiments [11]–[17]. In addition, many practical methods for realizing the PDC have been investigated also. For example, Woo *et al.* [18] utilized a phase locked loop for estimating the phase delay angle, and implemented it into a microprocessor. They experimentally verified that the efficiency of the BLDC motor could be improved by PDC. However, it is difficult to determine the optimum phase delay angle when an exogenous disturbance is applied to the motor, because it lacks the feedback information from the motor in their method. The phase advance circuit also have been proposed that removes the harmonic frequency. While most of the existing PDC methods improve the actuation performance and efficiency of BLDC motors at a high speed, they often deteriorate the motor performance at a low speed [19]. In addition, when the estimated phase delay is inaccurate, it is difficult to compensate for the actual phase delay effectively. In recent years, as sophisticated control devices, electric peripherals, and power devices have been improved dramatically, it has become able to develop a new PDC approach. For example, most studies are calculated the phase delay angle by analysis the waveform of phase current in commutation period [20]–[24]. Also, a linear model and a scaling factor for the phase advanced commutation were proposed in [25].

In this paper, a Fourier-series-based PDC is proposed for improving the output torque and power efficiency of a BLDC motor at high speeds. The proposed method utilizes an angular position sensor for detecting the phase advanced instance and uses the rotor angular speed as feedback information for calculating the required phase advance angle. The required phase advance angle, which is to compensate for the phase delay due to the inductance of motor windings, is calculated based on a transfer function consisting of the inductance and resistance of the motor windings. Then the transfer function is converted into its Fourier series for implementation. The proposed PDC method is realized by a digital logic circuit and a microprocessor, and its performance is verified through simulation and experimental results comparing with conventional BLDC motor driver systems.

II. Design of a Phase Delay Compensator (PDC) for BLDC Motors

A. Modeling of a BLDC Motor

The dynamic model of a three-phase BLDC motor driver is obtained for estimating the required phase advance angle to improve the actuation efficiency of the motor. Assuming that the resistance, R, the inductance, L, and the mutual inductance, M, are the same for the three windings, the dynamic response of the electric potential in the three windings can be modeled as a set of simple first order equations as follows [26]:

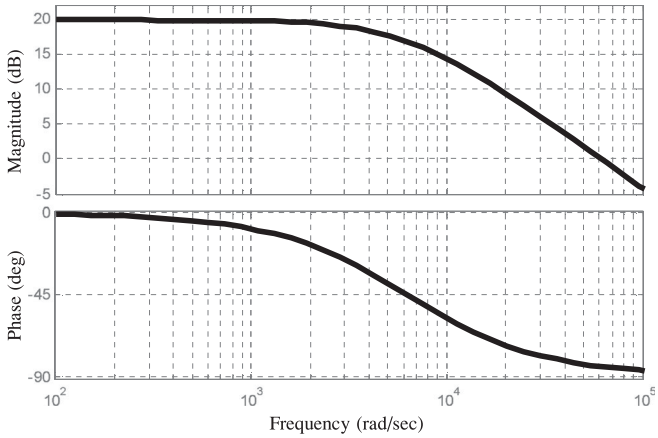

Fig. 2. Frequency response of the phase current in the motor winding of a BLDC motor.

$$\begin{bmatrix} v_u \\ v_v \\ v_w \end{bmatrix} = R \begin{bmatrix} i_u \\ i_v \\ i_w \end{bmatrix} + (L - M)\frac{d}{dt}\begin{bmatrix} i_u \\ i_v \\ i_w \end{bmatrix} + \begin{bmatrix} e_u \\ e_v \\ e_w \end{bmatrix} \quad (1)$$

where v and i are the phase voltage and phase current, respectively, and the subscripts, u, v, and w, represent the three phases. The back-electromotive force (EMF) of each phase, e_u, e_v, and e_w have trapezoidal shapes.

Ignoring the energy dissipation by heat, the electromagnetic power is to be totally transformed into the kinetic energy. Therefore, the electric motor torque can be obtained as

$$\tau_e = \frac{e_u i_u + e_v i_v + e_w i_w}{\omega_m} \quad (2)$$

where ω_m is the angular speed of a rotor. The electric motor torque in (2) can also be obtained from the fact that the torque and the current, and the angular speed and the back-EMF are proportionally related with each other. For more details, refer to [13].

When the moment of inertia, J, and viscous friction, B, are imposed on the rotor, the equation of mechanical motion is

$$J\frac{d\omega_m}{dt} + B\omega_m = \tau_e + \tau_L \quad (3)$$

where τ_L is an external torque applied to the rotor.

B. Efficiency Reduction by the Phase Delay

Taking the Laplace transformation of (1) for each winding, a transfer function of the electric relationship from effective phase voltage (i.e., phase voltage minus back-EMF) to the phase current (i.e., an output) can be obtained as

$$G(s) = \frac{1}{Ls + R} \quad (4)$$

where L and R are as defined in (1), and s is the Laplace operator. The mutual inductance, M, has been neglected because it is small compared to the inductance L in general [27]. Fig. 2 shows the frequency response of (4) with the actual parameters

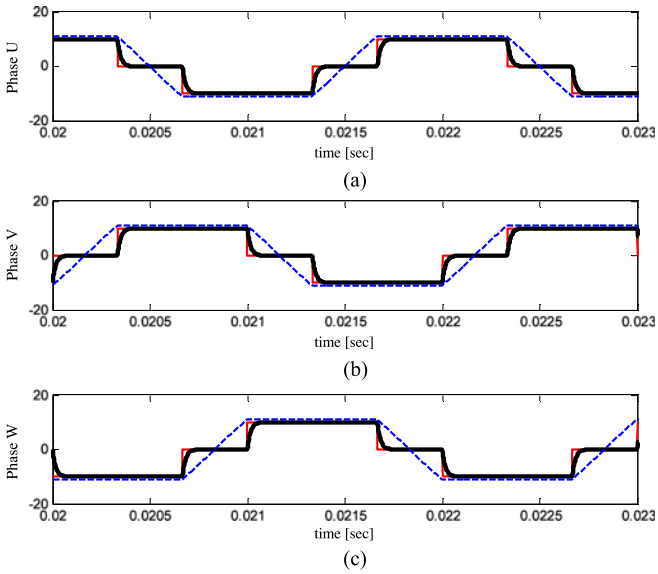

Fig. 3. Simulation result of the ideal phase current and real ideal phase current at a high speed: in (a)–(c), the dashed lines show the back-EMF, the continuous thin lines show the ideal phase current, and the continuous thick lines show the real phase current.

of a BLDC motor (EC-4pole 200W from Maxon Motor Company [28]). As shown in the figure, the phase current is to be delayed as the rotation speed of the rotor increases. Namely, the phase delay angle is increased as the switching rate of phase transition increases. The phase delay angle in the electric phase current can be calculated from the transfer function in (4), i.e.,

$$\phi(\omega) = \tan^{-1}\left(\frac{\mathrm{Im}(G(j\omega))}{\mathrm{Re}(G(j\omega))}\right) = \tan^{-1}\left(\frac{-L\omega}{R}\right) \tag{5}$$

where ω represents the frequency component of the electric phase current.

Fig. 3 shows the simulation result of the back-EMF, the ideal phase current without the phase delay, and the realistic phase current (i.e., one with the phase delay) at the maximum rotation speed of the EC-4pole BLDC motor [i.e., 16 000 revolutions per minute (r/min)]. The parameters are the same as in Fig. 2. Notice that the effective phase voltage applied to each winding has a quasi-square waveform, which is the case of most BLDC inverter systems [29]. When the phase current is delayed from the effective phase voltage due to the resistance and inductance of windings, as shown in Fig. 3, the magnetic field of the windings cannot be generated in phase with the back-EMF. This phase mismatch between the phase current and the back-EMF significantly reduces the output torque magnitude and the motor efficiency, which also limits the maximum speed of a BLDC motor.

C. Design of a Fourier-Series-Based PDC

In this section, a PDC method based on Fourier series is introduced. Since the shape of effective phase voltage applied to windings of a BLDC motor is not a sinusoidal waveform, (5) cannot be directly used for the design of a PDC algorithm. Therefore, the frequency components of the quasi-square waveform [29], which is similar to the effective phase voltage waveform, is obtained by Fourier series as follows:

$$v_a(t) = \frac{2}{\pi}\sum_{n=1}^{\infty}\frac{b_n}{n}\sin(n\omega_e t) \tag{6}$$

where the coefficient b_n is

$$b_n = \cos\left(\frac{n\pi}{6}\right) - \cos\left(\frac{5n\pi}{6}\right). \tag{7}$$

The phase current induced from the effective phase voltage in (6) in a winding can be calculated by (4), i.e.,

$$i(t) = \frac{2}{\pi}\sum_{n=1}^{\infty}\frac{b_n}{n}\frac{\sin(n\omega_e t + \phi(n\omega_e))}{\sqrt{L^2n^2\omega_e^2 + R^2}} \tag{8}$$

where $\phi(\bullet)$ is as in (5).

It should be noted that in most of the practical BLDC inverter systems, the only control variable in the inverter circuit is the triggering instance of the phase voltage, which is determined according to the change of hall sensor signals in general. Therefore, the phase delay in the induced phase current can be compensated by changing the triggering instance. Suppose that a new phase voltage, $v_{\mathrm{PDC}}(t) = v(t + dt)$, is applied to the motor windings by an inverter circuit. Then, the induced phase current is

$$i_{\mathrm{PDC}}(t) = \frac{2}{\pi}\sum_{n=1}^{\infty}\frac{b_n}{n}\frac{\sin(n\omega_e t + n\omega_e dt + \phi(n\omega_e))}{\sqrt{L^2n^2\omega_e^2 + R^2}}. \tag{9}$$

Therefore, if $dt = -\phi(n\omega_e)/n\omega_e$, the phase delay due to the resistance and inductance can be perfectly compensated. When the required time advance, dt, is determined considering only the first frequency component (i.e., $n = 1$), it may be set such that $dt = -\phi(\omega_e)/\omega_e = \tan^{-1}\left(\frac{L\omega_e}{R}\right)/\omega_e$. The effective phase voltage and phase current waveforms, however, include infinite frequency components as in (9), and, thus, dt should be determined considering as many frequency components as possible to effectively compensate for the phase delay.

In this paper, the time advance, dt, is obtained by a weighted summation of $-\phi(n\omega_e)/n\omega_e$ for $n = 1, 2, ..., N$, i.e.,

$$dt = \frac{1}{\omega_e}\sum_{n=1}^{N}\frac{c_n}{n}\tan^{-1}\left(\frac{nL\omega_e}{R}\right) \tag{10}$$

where N is a large number, and c_n's are weighting factors. It is reasonable to set c_n to be proportional to b_n in (7), because the larger the magnitude of a frequency component, the more influential the frequency component in the synthesized signal. In this aspect, the proposed coefficients are

$$c_n = \frac{|b_n|/n}{\sum_{k=1}^{N}|b_k|/k}. \tag{11}$$

Notice that the coefficients are scaled by $\left(\sum_{k=1}^{N}|b_k|/k\right)^{-1}$ in order to make $\sum_{n=1}^{N}c_n = 1$. By the scaling, $dt = \frac{1}{\omega_e}\tan^{-1}\left(\frac{L\omega_e}{R}\right)$ for $N = 1$, as desired. Given N, L, and R, the coefficients are deterministic and, thus, they can be calculated once any BLDC motor is selected. For example, for

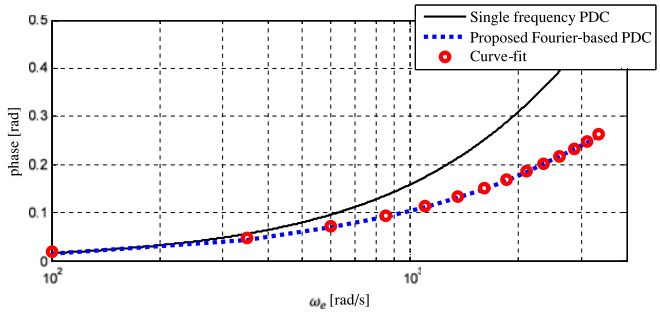

Fig. 4. Phase delay curves; the continuous line shows the single frequency case, the dashed line shows the phase delay calculated by the proposed Fourier-based PDC, and the circular markers show its curve-fit.

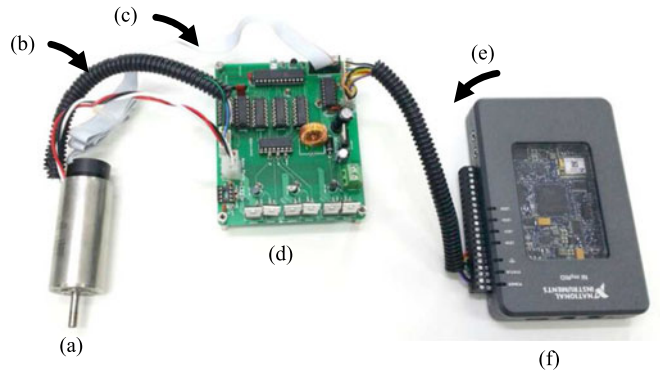

Fig. 5. A configuration of a BLDC motor system with the proposed PDC.

$N = 100$, the coefficients for the EC-4pole BLDC motor, which has $L = 0.0163$ mH and $R = 0.102\,\Omega$ [28], are $c_1 = 0.5216$, $c_3 = 0$, $c_5 = 0.1043$, $c_7 = 0.07451$, $c_9 = 0$,..., and $c_{2i} = 0$ for all $i = 1, 2, 3, ..., 50$.

For the implementation of the proposed PDC, the calculated time advance, dt, should be applied to the transition of phase voltages in advance to the hall sensor detection. In practice, however, it is not simple to apply the time advance to the control of the phase voltages, because dt is highly dependent on the rotation speed. For more convenient implementation of the proposed method, a *phase advance angle* is calculated from dt. Since the angular position of rotor can be easily estimated or measured by various methods, it is not difficult to apply the phase advance angle to a BLDC motor driver. The required phase advance angle is related with dt by the electrical angular speed, i.e.,

$$d\theta = \omega_e dt = \sum_{n=1}^{N} \frac{c_n}{n} \tan^{-1}\left(\frac{nL\omega_e}{R}\right) \tag{12}$$

where ω_e is an electrical angular speed. When a BLDC motor has only one set of three windings and one pair of magnet poles, the electrical angular speed is the same as the mechanical angular speed (i.e., $\omega_e = \omega_m$). When a motor has multiple sets of three windings, $\omega_e = p\omega_m$, where p is the number of pole pairs. Also, notice that the required phase advance angle in (12) is not scaled by $\frac{1}{\omega_e}$ unlike the time advance in (10), which makes the implementation of the proposed PDC simple.

In [18], the required phase advance angle was calculated by considering only the first frequency component of the phase voltage of BLDC motors. In a brushless alternating current motor system, its phase voltage and back-EMF are sinusoidal [30], and the single frequency assumption is reasonable. However, the effective phase voltage of BLDC motors has a quasi-square waveform and includes infinite frequency components. Therefore, the proposed method, which considers more frequency components compared to the conventional methods, may calculate the required phase advance angle more accurately. Fig. 4 shows the phase delay calculated for a single frequency component (i.e., the first harmonic frequency) and that obtained by the proposed method. Notice that the magnitudes of phase delays are different, which implies that the phase delay may be over-compensated if the single frequency is considered only.

Although the proposed phase advance angle can be calculated by (12), it includes the summation of a large number of components, which is a burden for a microprocessor in a motor driver. Recall that given N, R, and L, (12) is a function of ω_e only, and, thus, (12) can be simplified by a curve-fit; the proposed method can be simplified by utilizing a function

$$d\theta_a = k_1 \tan^{-1}\left(\frac{L\omega_e^{k_2}}{R}\right) \tag{13}$$

where k_1 and k_2 are constant coefficients to be obtained by the curve-fit. Notice that these parameters are determined according to the electrical parameters of a BLDC motor (i.e., L and R) and the number of frequency components. In practice, the authors have empirically found that 50 is large enough for N. Fig. 4 shows the phase advance angles calculated by (12) and (13). Notice that the curves match well, while (13) requires much less computation load.

D. BLDC Inverter Circuit for PDC

In order to realize the proposed PDC algorithm, an inverter circuit that enables switching the phase voltages according to the PDC signal, as well as the hall sensor signals, is necessary. Namely, a PDC inverter should be able to adjust the phase voltage transition instances according to the phase advance angle in (12) or (13). Therefore, the overall BLDC system with the proposed PDC requires the following three major components.

1) a BLDC motor with an incremental encoder and hall sensors [see in Fig. 5(a)];

2) a microprocessor that calculates the required phase advance angle, $d\theta$ or $d\theta_a$, and applies a PDC interrupt signal to the inverter circuit [see in Fig. 5(f)];

3) a PDC inverter that switches the U, V, and W phase voltages according to the hall sensor signals and the PDC interrupt signal [see in Fig. 5(d)].

Although the PDC inverter and the microprocessor are configured separately in Fig. 5, it is possible to realize both of them on one circuit board.

The phase transition in the phase voltage should be controlled according to the PDC interrupt signal, as well as the

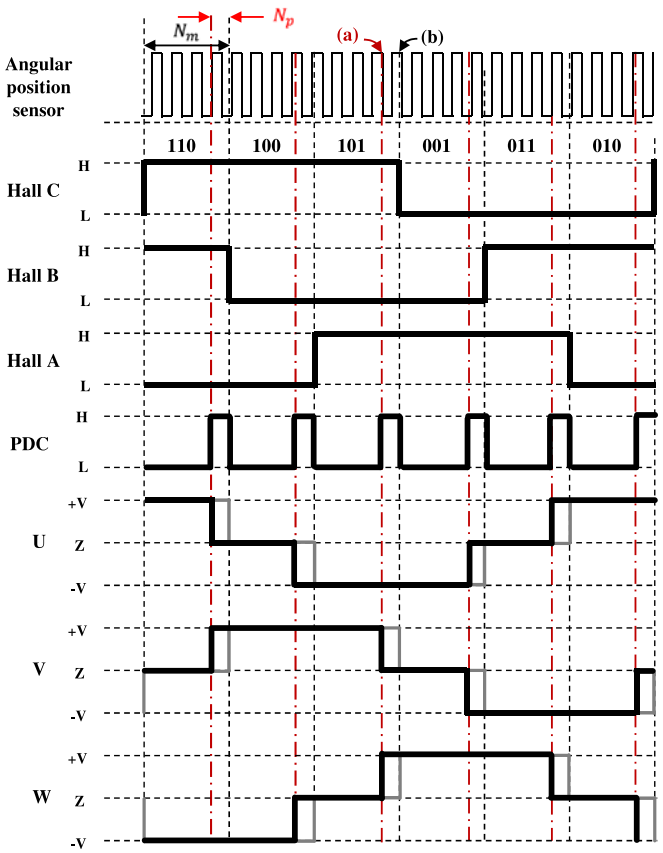

Fig. 6. Phase transitions in the U, V, and W with and without the proposed PDC; (a) shows the phase transition by the proposed PDC, and (b) shows phase transition by the hall sensor signals.

hall sensor signals. In the conventional BLDC motor driver systems, the phase voltages are determined such that $U+ = h_B \times \overline{h_A}, U- = \overline{h_B} \times h_A, V+ = h_C \times \overline{h_B}, V- = \overline{h_C} \times h_B$, $W+ = \overline{h_C} \times h_A$, and $W- = h_C \times \overline{h_A}$, where h_A, h_B, and h_C are the binary measurements of the hall sensors. In order to realize the proposed PDC, one more control variable is necessary such that the phase voltages can be controlled by the PDC. For this purpose, the microprocessor generates a PDC interrupt signal, P, which is a binary digital signal like the hall sensor signals. The proposed inverter logic with the PDC interrupt is

$$\begin{aligned} U+ &= \overline{P} \times h_B \times \overline{h_A} + P \times \overline{h_C} \times h_B \\ U- &= \overline{P} \times \overline{h_B} \times h_A + P \times h_C \times \overline{h_B} \\ V+ &= \overline{P} \times h_C \times \overline{h_B} + P \times h_C \times \overline{h_A} \\ V- &= \overline{P} \times \overline{h_C} \times h_B + P \times \overline{h_C} \times h_A \\ W+ &= \overline{P} \times \overline{h_C} \times h_A + P \times \overline{h_B} \times h_A \\ W- &= \overline{P} \times h_C \times \overline{h_A} + P \times h_B \times \overline{h_A}. \end{aligned} \tag{14}$$

Notice that the phase voltages are controlled not only by the hall sensor signals, but also by the PDC interrupt signal.

Fig. 6 shows an example of the hall sensor and PDC interrupt signals, and the corresponding switching sequences. The number of pulses in each step is constant, N_m, which is determined

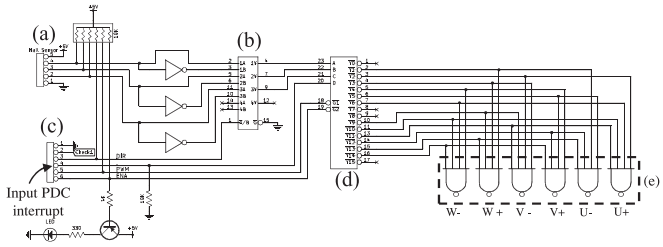

Fig. 7. Schematic digital logic circuit design for the proposed PDC driver.

by the poles of the motor. The number of pulses in Fig. 6(a) and (b), i.e., N_p, is calculated by (13). The PDC interrupt signals are determined by $N_m - N_p$, where the phase advance angle can be detected in advance to the hall sensor signal by an angular position sensor, such as an incremental encoder. The PDC interrupt signals are generated as shown in the figure, and the phase voltage transitions are adjusted according to the PDC interrupt signals following the inverter logic in (14). It should be noted that the proposed inverter logic in (14) is identical with the conventional inverter logics when the PDC interrupt signal is off.

In order to generate appropriate PDC interrupt signals for successful compensation of the phase delay of the electric phase currents, the phase advance angle is applied based on the angular position of the rotor, i.e.,

$$P = \begin{cases} 0, & \text{for } \frac{1}{3}(n-1)\pi \le d\hat{\theta}_e < \frac{1}{3}n\pi - d\theta_a \\ 1, & \text{for } \frac{1}{3}n\pi - d\theta_a \le d\hat{\theta}_e < \frac{1}{3}n\pi \end{cases} \tag{15}$$

for $n = 1, 2, 3, ...$, and $d\hat{\theta}_e$ is an incremental angle in terms of electrical phase. Since the electrical angular speed and the mechanical rotor speed are related by $\omega_e = p\omega_m$, where p is the number of pole pairs, $d\hat{\theta}_e$ can be obtained by $pd\hat{\theta}_m$, where $d\hat{\theta}_m$ is the incremental rotor angle measured from the last phase voltage transition instance. $d\hat{\theta}_m$ can be easily estimated by $d\hat{\theta}_m = \omega_m(t - t_0)$.

Fig. 7 shows a schematic circuit design for realizing the proposed PDC inverter logic. The hall sensors of a BLDC motor are connected to the circuit via a connector block (a). The hall sensor signals and their inverted signals are applied to a quadrature two-input multiplexer [see in Fig. 7(b)], which determines the direction of the rotor rotation. A number of commercialized chips are available for this purpose (e.g., see [31]). The outputs of the multiplexer and the PDC interrupt signal [see in Fig. 7(c)] are processed by a 4-line to 16-line demultiplexer (e.g., [32]) that generates twelve cases for selecting the phase voltages [see in Fig. 7(d)]. Finally, the six phase voltage inputs (i.e., $U+$, $U-$, $V+$, $V-$, $W+$, and $W-$) are determined by NAND logic gates based on the twelve cases generated by the demultiplexer [see in Fig. 7(e)]. The circuit design in Fig. 7 realizes the proposed inverter logic in (14). The outputs of the NAND gates are applied as the gate control signals of power MOSFETs for switching the phase voltages of a BLDC motor.

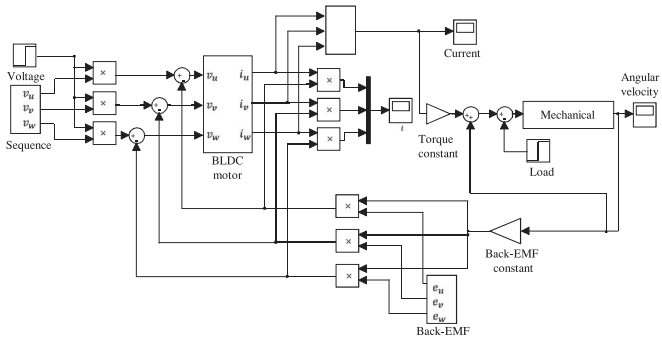

Fig. 8. Simulation block diagram of the proposed PDC for an EC-4pole BLDC motor.

TABLE I
SPECIFICATION OF A BLDC MOTOR USED IN EXPERIMENTS [28]

Specification	Value [unit]
Nominal voltage	24 [V]
Nominal current	10.5 [A]
Nominal speed	15900 [r/min]
Nominal torque	135 [mN·m]
Terminal resistance	0.102 [Ω]
Terminal inductance	0.0163 [mH]
Max. efficiency	89 [%]

III. SIMULATION STUDY

A. Simulation Setup

The BLDC system driven by the proposed PDC was first verified by simulation studies with a commercialized simulation toolbox, as shown in Fig. 8. The simulation model consisted of three parts: the equations of electric motions in (1), the equations of mechanical motions in (2) and (3), and a load (i.e., disturbance torque, τ_L). The simulation parameters were the same as the actual motor system listed in Table I.

In order to implement the proposed PDC, the phase advance angle should be obtained as in (12) prior to obtaining the simplified method in (13). For the selected motor, the electrical parameters were obtained from the specification, as in Table I, and N was set to a sufficiently large number ($N = 100$). After obtaining the phase advance angle by (12), a curve-fit was obtained with the basis function of (13). The obtained parameters were $k_1 = 3.346$ and $k_2 = 0.760$, i.e.,

$$d\theta_a = 3.346 \tan^{-1}\left(1.598 \times 10^{-4} \omega_e^{0.760}\right). \quad (16)$$

B. Phase Delay Compensation

Fig. 9 shows the simulation results of the proposed PDC with the physical parameters of EC-4pole 200 W BLDC motor. The results are compared with conventional methods. Fig. 9 shows the simulated phase current in one of the three motor windings. Notice that the time delay in the phase current, which was due to the resistance and inductance of the motor winding, was compensated by the proposed PDC. When the BLDC motor is controlled by PDC, switching devices activate at the edge of

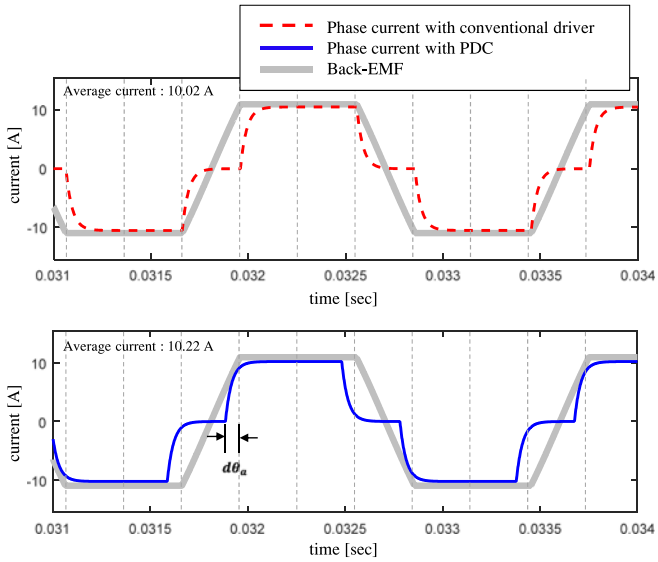

Fig. 9. Simulation results of the phase current at 16000 r/min.

the trapezoidal back-EMF, and the corresponding phase current increases rapidly based on (1). In the same manner, the end of the flat top of trapezoidal, switching devices deactivate and the phase current decreases rapidly. Therefore, the magnitude of the phase current was significantly increased where the back-EMF is flat [e.g., see the dashed line in the figure]. This implies that the electric power can be significantly improved, because the electromagnetic power is defined by the multiplication of the back-EMF and the phase current.

IV. EXPERIMENTAL VERIFICATIONS

In this section, the performance and effectiveness of the proposed PDC are verified through experimental results.

A. Experimental Setup

The proposed PDC algorithm and the inverter circuit can be applied to any BLDC motor, as long as it is equipped with an incremental encoder. In this paper, an EC-4pole 200 W BLDC motor was utilized for performance verification. The specification of the selected motor is shown in Table I.

An experimental test-bed was set, as shown in Figs. 5 and 10. NI myRIO-1900, an FPGA board manufactured by National Instrument Company, was utilized as a microprocessor for calculating the phase advance angle in real-time. In order to generate the PDC interrupt signal according to the phase advance angle calculated by (16), an incremental encoder installed at the BLDC motor was utilized. The utilized encoder has the resolution of 2000 pulses per revolution, and the selected motor has four poles (i.e., two pairs of poles, $p = 2$), which implies that 1000 pulses represent one electrical revolution. In addition, each electrical revolution has six steps, as shown in Fig. 1, and thus each step length is about 167 encoder pulses. The unit of the calculated phase advance angle is radians in the electrical revolution domain, which means that the PDC implemented

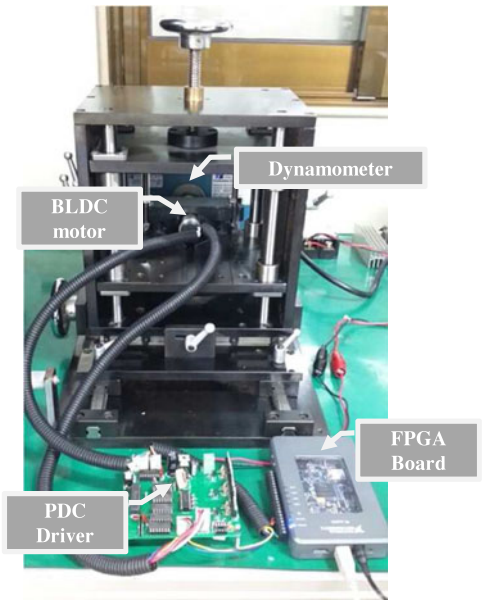

Fig. 10. Experimental setup for verification of PDC using incremental encoder.

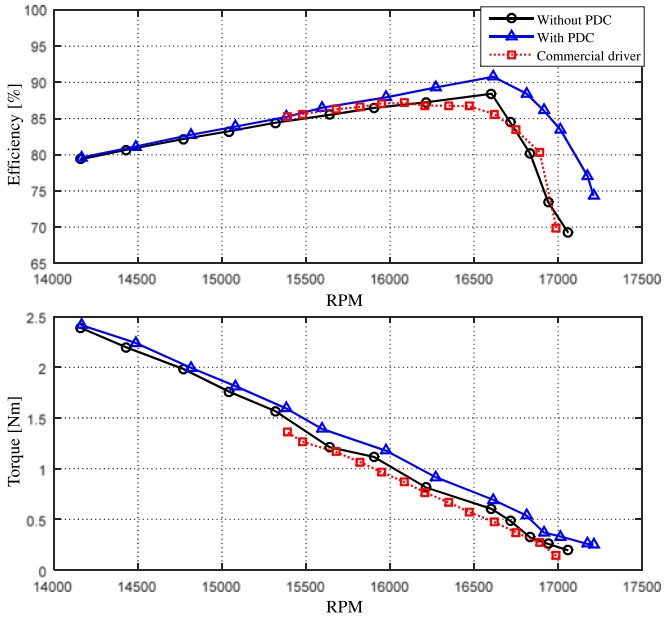

Fig. 11. Efficiency and torque of the BLDC motor according to angular speeds with and without PDC.

for the selected motor has the resolution of $2\pi/1,000 = 6.28 \times 10^{-3}$ rad.

A dynamometer, which measures the rotational speed, the output torque, the electric power, and the operation efficiency, was utilized as shown in Fig. 10. By the dynamometer, the efficiency of the selected BLDC motor driven by the proposed PDC algorithm and circuit could be accurately measured and analyzed. In order to verify the efficiency of the BLDC system, the rotor of the motor was imposed by a load controlled by the dynamometer. The dynamometer was controlled such that the phase current was increased from the unloaded current to the maximum allowable current (i.e., 20 A).

B. Motor Efficiency and Power

The motor power efficiency, η, is calculated as $\eta = \tau_e \omega_m / VI \times 100$, where the supply voltage was $V = 24$ V in the experiments. The maximum supply current was set to 20A by a dc power supply.

Fig. 11 shows the efficiencies and torque of the BLDC motor driven by the proposed inverter circuit shown in Fig. 7 with and without the proposed PDC algorithm. For more objective verification, a commercialized motor driver, ESCON 50/5 of the Maxon Motor Company [33], was also tested. In the three experimental settings, i.e.,

1) the proposed inverter with the PDC interrupt signal;
2) the same circuit without the PDC interrupt signal;
3) the ESCON 50/5 commercialized driver;

the other experimental conditions (e.g., the supply voltage, the maximum current limit, the control input signal, the feedback condition, etc.) were all identical except for the inverter settings.

The change of the motor power efficiency was observed while changing the load by the dynamometer. Before measuring the efficiency for each of the three experimental settings, the BLDC motor was run without any load. Once the motor reached its maximum no-load speed, the dynamometer started measuring the motor power efficiency with respect to the angular speed by changing (i.e., increasing) the load. It should be first noted that the maximum no-load speed was improved from 17,061 to 17,221 r/min by the PDC, which also implied the increased output torque.

It is also noteworthy that without the PDC interrupt signal, the proposed system in Fig. 7 and the commercialized driver showed similar performance [see the square and circular markers in Fig. 11], which implies that the proposed inverter circuit with the multiplexer and demultiplexer did not deteriorate the motor operation performance. When the proposed PDC algorithm was activated, the motor power efficiency was increased significantly [see the triangular markers in the figure] in particular at high angular speeds. This was because the phase delay in the induced phase current affected the motor efficiency more significantly at the high angular speeds. When the angular speed was low, the motor efficiencies for the three experimental settings were similar. Notice that the motor efficiency of the motor was increased from 69.4% to 83.1% at 17 000 r/min by the proposed PDC algorithm, which was about 13.7% increase. Also, the output torque was increased from 0.139 to 0.341 N·m at 17,000 r/min by the PDC. The experimental results in Fig. 11 showed that the proposed PDC method could increase the output torque and improve the motor efficiency, as well as the maximum angular speed.

C. Position Tracking Control

For the performance verification of the proposed PDC algorithm and inverter circuit in a more practical setting, a position tracking control system was set, as shown in Fig. 12. The overall control system consisted the following four major components.

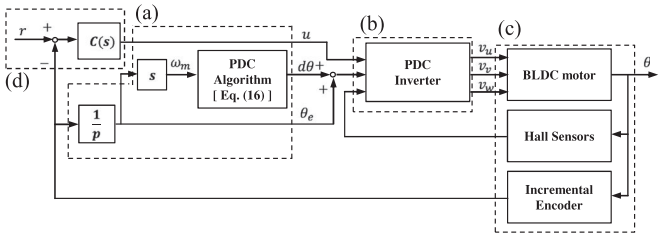

Fig. 12. Block diagram for position-tracking control with the proposed PDC driver.

1) the PDC algorithm that calculates the phase advance angle [see in Fig. 13(a)];

2) the PDC inverter circuit that controls the phase voltages according to the PDC interrupt signal and the hall sensor signals [see in Fig. 13(b)];

3) a BLDC motor equipped with an incremental encoder and hall sensors [see in Fig. 13(c)];

4) a position tracking controller [see in Fig. 13(d)].

In the experiments, the position tracking controller and the PDC algorithm were implemented in the same microprocessor, NI-myRIO 1900, with the sampling frequency of 1 kHz. The PDC interrupt signal was generated at the FPGA level with the sampling frequency of 40 MHz. In the figure, s represents the Laplace operator, and p is the number of pole pairs. For the EC-4pole 200W BLDC motor used in the experiments, $p = 2$. The phase advance angle, $d\theta$, was calculated by the simplified function in (16). Also, $C(s)$ is a simple proportional-integrative-derivative (PID) controller

$$C(s) = \frac{K_d s^2 + K_p s + K_i}{s} \tag{17}$$

where the controller gains were $K_p = 2800$, $K_i = 40$, and $K_d = 420$. The reference trajectory was set to

$$r(t) = 160\pi \text{sgn}(\sin(0.5\pi t)) \tag{18}$$

which requires 160 revolutions within 2 s. The reference trajectory was designed to observe a high speed rotation at its transient response and a low speed rotation after the transient.

Fig. 13 shows the experimental result of the position tracking control with and without the PDC algorithm. The other conditions, including the inverter circuit and PID controller gains, were all identical. The motor was controlled to alternate its angular position between $+80$ and -80 revolutions, as in (18).

Both the experimental settings, i.e., the overall control loop with and without the PDC algorithm, showed similar performances, as shown in Fig. 13(a). In the zoomed-in graphs shown in Fig. 13(b) and (c), however, the improvement of the motor power efficiency is clearly shown. The phase advance angle required for compensating the phase delay in the phase current was calculated in real-time, as shown in Fig. 13(a). Since the phase advance angle was a function of the angular speed as in (16), the calculated phase advance was proportionally related to the angular speed of rotor, as shown in the figure. Notice from Fig. 13(c) that the magnitude of the generated control input was reduced when the phase delay was compensated by the

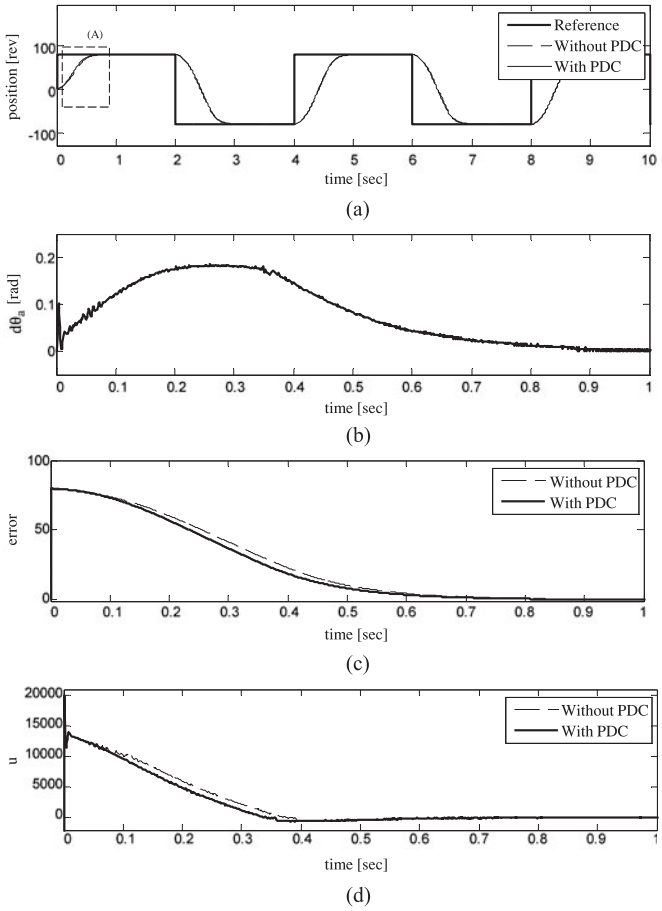

Fig. 13. The trajectory tracking performance with and without the PDC algorithm ((a) the reference trajectory and position-tracking control with and without PDC algorithm, (b) the calculated phase advance angle, $d\theta_a$, by the PDC algorithm, (c) the control input u with and without PDC, (d) the tracking errors with and without the PDC algorithm).

proposed PDC algorithm. The second norm values of $u(t)$'s over one period (i.e., from 0 to 2 s) showed that the control input was reduced by 13.69% by the PDC algorithm. This was because when the phase delay in the phase current was not compensated, a larger actuation power was necessary due to the asynchronism between the back-EMF and the phase current.

It is also noteworthy that although the generated control input was reduced by the PDC algorithm, nevertheless the tracking performance with the PDC algorithm was even improved, as shown in the Fig. 13(c); the tracking error was reduced when the PDC algorithm was activated.

For more objective comparison, a linear quadratic (LQ) performance index, which consists of the quadratic terms of the tracking error, $e(t)$, and the control input, $u(t)$, was utilized, i.e.,

$$J = \int_0^T [e^2(t) + ru^2(t)]dt \tag{19}$$

where r is a weight factor that balances the two terms, and T is the experimental time span. The LQ performance index evaluates both the tracking control performance and the energy

efficiency at the same time. The LQ performance index of the experimental result with the proposed PDC was remarkably smaller than that without PDC; the value of J was reduced by 1.25% by the PDC algorithm during the entire experiment (i.e., from $T = 0$ to $T = 10$ in Fig. 13). This implies that a feedback control system of a BLDC motor with the proposed PDC shows better energy efficiency and tracking control performance.

V. Conclusion

In this paper, the efficiency reduction problem of BLDC motors was investigated in the viewpoint of electric phase delay in motor windings due to their inductance and resistance, and the PDC was proposed to address this problem. Also, quasi-square waveform of phase current delay in BLDC motor is ambiguous to determine quantitatively. In order to compensate for the phase delay due to the inductance and resistance of BLDC motor windings, a phase advance angle was determined based on the Fourier series of the phase voltage waveform that sum of simple sine waves. For implementation of the proposed algorithm in real-time, a simplified method was also introduced, that is logic circuit design for rapid operation. Also, a customized BLDC inverter circuit was designed. Since the only control variable for compensating the phase delay by the inverter circuit was the triggering instance of the phase voltage, the inverter circuit was designed such that it was able to switch the phase voltages according to a PDC interrupt signal generated by the PDC algorithm, as well as hall sensor signals of the motor.

The proposed PDC algorithm and the inverter circuit were verified by simulations and experiments. In the experiments, a dynamometer was utilized for objectively evaluating the motor output power and efficiency of a BLDC motor with and without the proposed PDC method. Since the PDC method compensates the mismatch of delayed phase current and electromagnetic force, the slope of phase current increases rapidly. As a result, the output torque and the motor efficiency were improved in particular at high angular speeds. The maximum angular speed of the motor could also be increased by the proposed method. The improved efficiency was also observed in a feedback control experiment; the proposed PDC improved the tracking control performance with less control input.

References

[1] C.-H. Chen and M.-Y. Cheng, "A new cost effective sensorless commutation method for brushless dc motors without phase shift circuit and neutral voltage," *IEEE Trans. Power Electron.*, vol. 22, no. 2, pp. 644–653, Mar. 2007.

[2] J. Shao, "An improved microcontroller-based sensorless brushless DC (BLDC) motor drive for automotive applications," *IEEE Trans. Ind. Appl.*, vol. 42, no. 5, pp. 1216–1221, Sep. 2006.

[3] D.-D. Nguyen and M. C. Ta, "New direct Torque control scheme for BLDC motor drives suitable for EV applications," in *Proc. IEEE Veh. Power Propulsion Conf.*, Oct. 2014, pp. 1–5.

[4] M. Z. Youssef, "Design and performance of a cost-effective BLDC drive for water pump application," *IEEE Trans. Ind. Electron.*, vol. 62, no. 5, pp. 3277–3284, May 2015.

[5] N. Parspour and R. Hanitsch, "Fuzzy controlled brushless DC motor for medical applications," in *Proc. 20th Int. Conf. Ind. Electron., Control Instrum.*, Sep. 1994, vol. 2, pp. 1310–1314.

[6] W. H. Sakman, "A brushless DC motor controlled by a microprocessor with examples for a three-phase motor," *IEEE Trans. Ind. Electron.*, vol. IE-34, no. 3, pp. 339–344, Aug. 1987.

[7] G. H. Jang and M. G. Kim, "Optimal commutation of a BLDC motor by utilizing the symmetric terminal voltage," *IEEE Trans. Magn.*, vol. 42, no. 10, pp. 3473–3475, Oct. 2006.

[8] D.-K. Kim, K.-W. Lee, and B.-Il Kwon, "Commutation torque ripple reduction in a position sensorless brushless DC motor drive," *IEEE Trans. Power Electron.*, vol. 21, no. 6, pp. 1762–1768, Nov. 2006.

[9] Y.-S. Lai, F.-S. Shyu, C.-W. Lin, and W.-S. Chang, "Novel torque boost technique for brushless DC motor drives without current sensor," in *Proc. 2004 IEEE Annu. Conf. Ind. Electron. Soc.*, Nov. 2004, pp. 2870–2873.

[10] J.-J. Moon, W.-S. Im, and J.-M. Kim, "Novel phase advance method of BLDC motors for wide range speed operations," in *Proc. IEEE Appl. Power Electron. Conf. Expo.*, 2013, pp. 2343–2348.

[11] S. K. Safi, P. P. Acarnley, and A. G. Jack, "Analysis and simulation of the high-speed torque performance of brushless DC motor drives," *Inst. Electr. Eng. Proc. Elect. Power Appl.*, vol. 142, no. 3, pp. 191–200, May 1995.

[12] C. C. Chan, J. Z. Jiang, W. Xia, and K. T. Chau, "Novel wide range speed control of permanent magnet brushless motor drives," *IEEE Trans. Power Electron.*, vol. 10, no. 5, pp. 539–546, Sep. 1995.

[13] T.-Y. Lee, J.-Y. Song, J. Kim, Y.-J. Kim, S.-Y. Jung, and J.-M. Je, "Phase advance control to reduce torque ripple of brush-less DC motor according to winding connection, wye and delta," *J. Electr. Eng. Technol.*, vol. 9, no. 6, pp. 2201–2208, 2014.

[14] N. Z. Yahaya, M. N. Abu-Bakar, and M. S. Mohd, "Study of phase advance angle control (PAAC) technique for brushless DC (BLDC) motor," in *Proc. 2nd IEEE Conf. Control, Syst. Ind. Inform.*, Jun. 2013, pp. 71–75.

[15] S.-J. Lee, J.-P. Hong, and W.-K. Jang, "Characteristics comparison of BLDC motor according to the lead angles," in *Proc. IEEE Veh. Power Propulsion Conf.*, Oct. 2012, pp. 879–883.

[16] C.-G. Kim, J.-H. Lee, H.-W. Kim, and M.-J. Youn, "Study on maximum torque generation for sensorless controlled brushless DC motor with trapezoidal back EMF," *Inst. Electr. Eng. Proc. Elect. Power Appl.*, vol. 152, no. 2, pp. 277–291, Mar. 2005.

[17] S.-I. Park, T.-S. Kim, S.-C. Ahn, and D.-S. Hyun, "An improved current control method for torque improvement of high-speed BLDC motor," in *Proc. IEEE Appl. Power Electron. Conf. Expo.*, 2003, vol. 1, pp. 294–299.

[18] K.-j. Woo, S.-K. Chang, and H.-C. Lee, "Driving characteristics improvement of brushless DC motor by commutation angle control," *J. Korean Inst. Illuminating Electr.*, vol. 4, no. 3, pp. 50–58, Sep. 1990.

[19] A. Tozune and T. Takeuchi, "Improvement of torque-speed characteristics of brushless motor by automatic lead angle adjustment," *Int. Power Electron. Motion Control Conf.*, Aug. 2004, vol. 2, pp. 583–587.

[20] W.-S. Im, J.-P. Kim, J.-M. Kim, and K.-R. Baek, "Torque maximization control of 3-phase BLDC motors in the high speed region," *J. Power Electron.*, vol. 10, no. 6, pp. 717–723, Nov. 2010.

[21] C. Shin, C. Choi, and W. Lee, "Advance angle calculation for improvement of the torque-to-current ratio of brushless DC motor drives," in *Proc. Int. Conf. Adv. Electr. Electron. Eng.*, 2012, pp. 1410–1414.

[22] B.-G. Gu, J.-H. Choi, and I.-S. Jung, "Simple lead angle adjustment method for brushless DC motors," *J. Power Electron.*, vol. 14, no. 3, pp. 541–548, May 2014.

[23] B. M. Nguyen and M. C. Ta, "Phase advance approach to expand the speed range of brushless DC motor," in *Proc. 7th IEEE Int. Conf. Power Electron. Drive Syst.*, Nov. 2007, pp. 1255–1262.

[24] J.-H. Choi, J. S. Park, J.-H. Kim, and I.-S. Jung, "Control scheme for efficiency improvement of slim type BLDC motor," in *Proc. Int. Symp. Power Electron., Electr. Drives, Autom. Motion*, Jun. 2014, pp. 820–824.

[25] S.-M. Sue, K.-L. Wu, J.-S. Syu, and K.-C. Lee, "A phase advanced commutation scheme for IPM-BLDC motor drives," in *Proc. 4th IEEE Conf. Ind. Electron. Appl.*, May 2009, pp. 2010–2013.

[26] P. Pillay and R. Krishnan, "Modeling, simulation, and analysis of permanent-magnet motor drives, Part II: The brushless DC motor drive," *IEEE Trans. Ind. Appl.*, vol. 2, no. 3, pp. 575–578, Mar./Apr. 2001.

[27] A. G. Jack, B. C. Mecrow, and J. A. Haylock, "A comparative study of permanent magnet and switched reluctance motors for high-performance fault-tolerant applications," *IEEE Trans. Ind. Appl.*, vol. 32, no. 4, pp. 889–895, Jul./Aug. 1996.

[28] Maxon Motor Ag., "Maxon Motor." 2013. [Online]. Available: http://www.maxonmotor.com

[29] T. M. Jahns, "Torque production in permanent-magnet synchronous motor drives with rectangular current excitation," *IEEE Trans. Ind. Appl.*, vol. IA-20, no. 4, pp. 803–813, Jul./Aug. 1984.

[30] J. R. Hendershort, Jr and T. J. E. Miller, *Design of Brushless Permanent-Magnet Motors.* Oxford, U.K.: Clarendon, 1994.
[31] Texas Instruments, "High-Speed CMOS Logic Quad 2-Input Multiplexers," 74HC157 datasheet, Sep. 1997. [Revised Oct. 2003].
[32] Texas Instruments, "High-Speed CMOS Logic 4- to 16-Line Decoder/Demultiplexer," 74HC154 datasheet, Sep. 1997. [Revised Jun. 2004].
[33] Maxon Motor Ag., "ESCON 50/5 Servo Controller P/N 409510," Hardware Reference, Sep. 2013.
[34] R. Carlson, M. Lajoie-Mazenc, and J. C. D. S. Fagundes, "Analysis of torque ripple due to phase commutation in brushless dc machines," *IEEE Trans. Ind. Appl.*, vol. 28, no. 3, pp. 632.638, May/Jun. 1992.

Myougseok Lee (S'17) received the B.Eng. degree in mechanical engineering in 2014, and the M.S. degree in mechanical engineering in 2016 both from Sogang University, Seoul, South Korea.

In 2016, he joined the Hyundai Motors, where he is currently an Research Engineer. His research interests include BLDC motor driver and its application to control.

Kyoungchul Kong (S'4–M'9) received the B.Eng. degree in mechanical engineering (summa cum laude) in 2004, the B.S. degree in physics in 2004, and the M.S. degree in mechanical engineering in 2006, all from Sogang University, Seoul, South Korea, and the Ph.D. degree in mechanical engineering from the University of California, Berkeley, CA, USA, in 2009.

In 2011, he joined the Department of Mechanical Engineering, Sogang University, Seoul, South Korea. He has authored or coauthored more than 100 technical articles in journals and conference proceedings in the area of mechatronics, including locomotive robotics and human robot interactive systems. His current research interests include design, modeling, and control of mechatronic systems with emphasis on locomotion and mobility of robotic systems.

Dr. Kong received the Bronze Medal of Cybathlon 2016, the Young Researcher Award of IFAC Mechatronics TC in 2016, the Hakbo Assistive Robotics Technology Award of KROS in 2016, and many others.